Abstracta

Ano XXI - N. 04

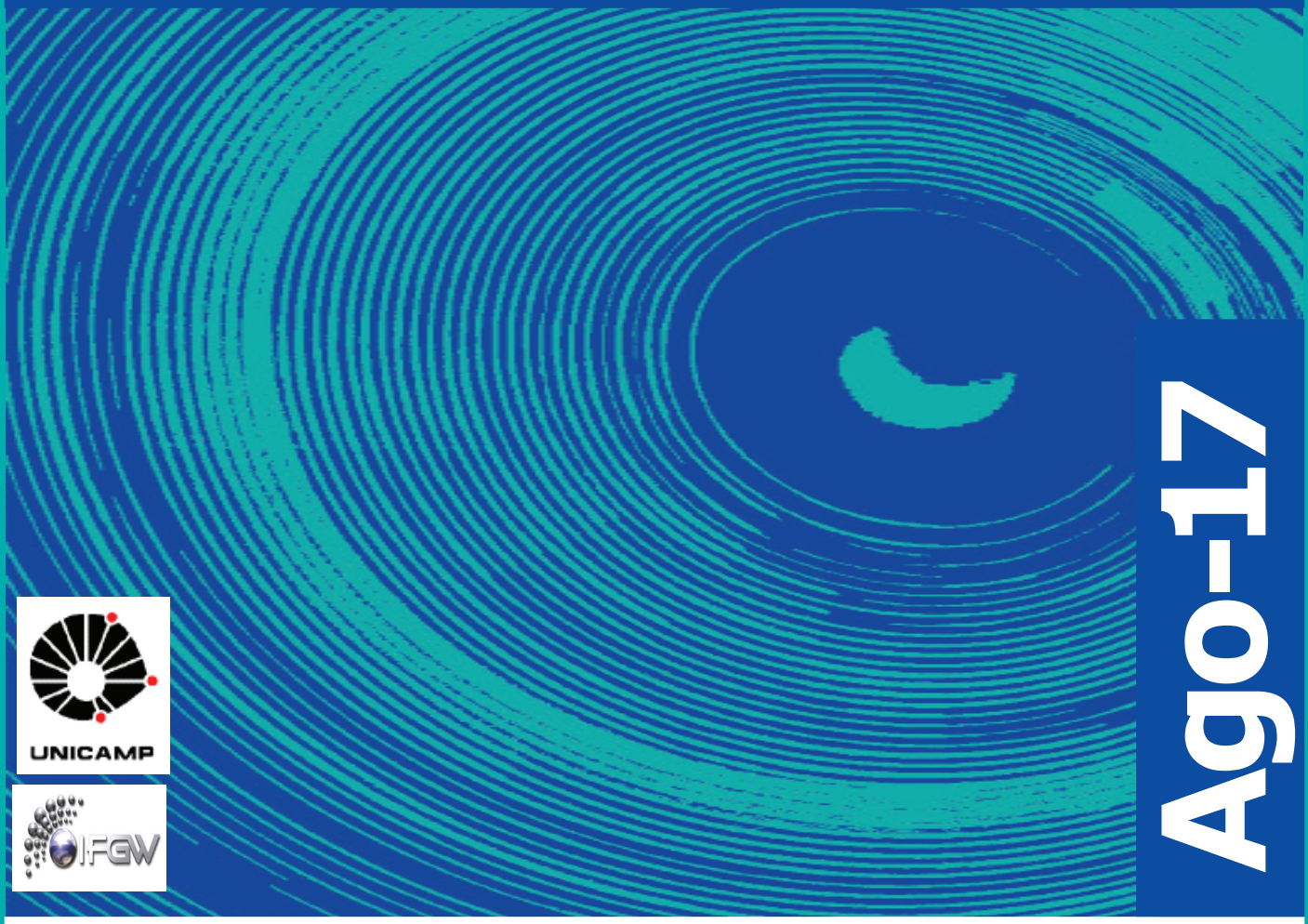

Ago-17

UNICAMP

IFGW

Artigos publicados

[P126-2017] "A search for new phenomena in pp collisions at root s=13TeV in final states with missing transverse momentum and at least one jet using the alpha(T) variable"

Khachatryan, V.; Sirunyan, A. M.; Tumasyan, A.; **Chinellato, J. A.*; Tonelli Manganote, E. J.*;** et al.
CMS Collaboration

A search for new phenomena is performed in final states containing one or more jets and an imbalance in transverse momentum in pp collisions at a centre-of-mass energy of 13 TeV. The analysed data sample, recorded with the CMS detector at the CERN LHC, corresponds to an integrated luminosity of 2.3 fb(-1). Several kinematic variables are employed to suppress the dominant background, multijet production, as well as to discriminate between other standard model and new physics processes. The search provides sensitivity to a broad range of new-physics models that yield a stable weakly interacting massive particle. The number of observed candidate events is found to agree with the expected contributions from standard model processes, and the result is interpreted in the mass parameter space of fourteen simplified supersymmetric models that assume the pair production of gluinos or squarks and a range of decay modes. For models that assume gluino pair production, masses up to 1575 and 975 GeV are excluded for gluinos and neutralinos, respectively. For models involving the pair production of top squarks and compressed mass spectra, top squark masses up to 400 GeV are excluded.

EUROPEAN PHYSICAL JOURNAL C 77[5], 294, 2017. DOI: 10.1140/epjc/s10052-017-4787-8

[P127-2017] "Anharmonic rattling vibrations effects in the ESR of Er3+ doped SmB6 Kondo insulator"

Lesseux, G. G.*; Rosa, P. F. S.; Fisk, Z.; Schlottmann, P.; **Pagliuso, P. G.*; Urbano, R. R.*; Rettori, C.***

We report X-band Electron Spin Resonance (ESR) experiments on approximate to 0.2% and approximate to 0.7% Er3+ doped SmB6 at low temperature (4 K - 40 K). The crystal field ground state of Er3+ in SmB6 is a 8 quartet with a nearby Gamma(6) excited doublet. The angular dependence of the resonances is not consistent with transitions between pure cubic crystal field states. The data were interpreted in terms of a dynamic Jahn-Teller (JT) effect by a coupling to Gamma(3) vibrational modes, which we propose to originate from the rattling of the small Er3+ ions in the large SmB6 cage. Our data show an anisotropic pair of E and E' resonances at g approximate to 4.4 and two nearly isotropic signals at g approximate to 5.8, one intense and narrow (A vibrational mode) and the other broad and faint, which we attribute to Er3+ ions at lattice sites which are strongly affected by strain, defects and/or extrinsic Al impurities that inhibits the JT effects. Our results are in general consistent with those previously reported by Sturm et al. In addition to the angular dependence of the lines, we discuss the intensities, g-values and the linewidths of the Er3+ transitions as a function of temperature.

AIP ADVANCES 7[5], 055709, 2017. DOI: 10.1063/1.4974914

[P128-2017] "Azimuthally Differential Pion Femtoscopy in Pb-Pb Collisions at root s(NN)=2.76 TeV"

Adamova, D.; Aggarwal, M. M.; **Albuquerque, D. S. D.*; Chinellato, D. D.*; De Souza, R. D.*; Takahashi, J.*;** et al.
ALICE Collaboration

We present the first azimuthally differential measurements of the pion source size relative to the second harmonic event plane in Pb-Pb collisions at a center-of-mass energy per nucleon-nucleon pair of root(NN)-N-s = 2.76 TeV. The measurements have been performed in the centrality range 0%-50% and for pion pair transverse momenta 0.2 < k(T) < 0.7 GeV/c. We find that the R-side and R-out radii, which characterize the pion source size in the directions perpendicular and parallel to the pion transverse momentum, oscillate out of phase, similar to what was observed at the Relativistic Heavy Ion Collider. The final-state source eccentricity, estimated via R-side oscillations, is found to be significantly smaller than the initial-state source eccentricity, but remains positive-indicating that even after a stronger expansion in the in-plane direction, the pion source at the freeze-out is still elongated in the out-of-plane direction. The 3 + 1D hydrodynamic calculations are in qualitative agreement with observed centrality and transverse momentum R-side oscillations, but systematically underestimate the oscillation magnitude.

PHYSICAL REVIEW LETTERS 118[22], 222301, 2017. DOI: **10.1103/PhysRevLett.118.222301**

[P129-2017] "Calculation of lineal energies for water and DNA bases using the Rudd model cross sections integrated within the Geant4-DNA processes"

Francis, Z.; El Bitar, Z.; Incerti, S.; **Bernal, M. A.*;** Karamitros, M.; Tran, H. N.

This study presents new parameters for proton ionisation cross sections in guanine, adenine, thymine, and cytosine based upon the semi-empirical Rudd model. The same model was used to find differential electron cross sections considering a speed scaling procedure. To accelerate computation, the total electron cross sections were obtained using the binary-encounter-Bethe approximation instead of the integrated Rudd formula. The cross sections were implemented in the Geant4 simulation toolkit as Geant4-DNA processes, and simulations were carried out measuring protons lineal energies in spherical micrometric volumes filled with water, adenine, thymine, guanine, and cytosine. Large differences were seen in the lineal energies evaluated for the different materials, with the lineal energy measured in guanine being sometimes twice that of water. This suggests that the cross sections developed here should be considered in biological simulations where cellular substructures are modelled, in contrast to the current approach which approximates these volumes as consisting of liquid water.

JOURNAL OF APPLIED PHYSICS 122[1], 014701, 2017. DOI: 10.1063/1.4990293

[P130-2017] "Cathodoluminescence in the scanning transmission electron microscope"

Kociak, M.; **Zagonel, L. F.***

Cathodoluminescence (CL) is a powerful tool for the investigation of optical properties of materials. In recent years, its combination with scanning transmission electron microscopy (STEM) has demonstrated great success in unveiling new physics in the field of plasmonics and quantum emitters. Most of these results were not imaginable even twenty years ago, due to conceptual and technical limitations. The purpose of this review is to present the recent advances that broke these limitations, and the new possibilities offered by the modern STEM-CL technique. We first introduce the different STEM-CL operating modes and the technical specificities in STEM-CL instrumentation. Two main classes of optical excitations, namely the coherent one (typically plasmons) and the incoherent one (typically light emission from quantum emitters) are investigated with STEM-CL.

For these two main classes, we describe both the physics of light production under electron beam irradiation and the physical basis for interpreting STEM-CL experiments. We then compare STEM-CL with its better known sister techniques: scanning electron microscope CL, photoluminescence, and electron energy-loss spectroscopy. We finish by comprehensively reviewing recent STEM-CL applications.

ULTRAMICROSCOPY 176(SI), 112-131, 2017. DOI: 10.1016/j.ultramic.2017.03.014

[P131-2017] "Coherent frequency combs for spectroscopy across the 3-5 mu m region"

Maser, D. L.; Ycas, G.; **Depetri, W. I.*; Cruz, F. C.***; Diddams, S. A.

A tunable mid-infrared frequency comb was created via difference frequency generation. Pulses between 1 and 1.5 mu m were mixed to generate light ranging from 2.6 to 5.2 mu m. Two such combs were heterodyned at 5 mu m to show their coherence and potential for spectroscopy. The properties of the comb were modeled using numerical simulation, which confirmed the observed bandwidths.

APPLIED PHYSICS B-LASERS AND OPTICS 123[4], 142, 2017. DOI: 10.1007/s00340-017-6714-y

[P132-2017] "Combined fit of spectrum and composition data as measured by the Pierre Auger Observatory"

Aab, A.; Abreu, P.; Aglietta, M.; **Chinellato, J. A.*; Daniel, B.*; Diaz Castro, M. L.*; Dobrigkeit, C.*; Fauth, A. C.*; Kemp, E.*; Muller, M. A.*; Pereira, L. A. S.*; Theodoro, V. M.***; et al. Pierre Auger Collaboration

We present a combined fit of a simple astrophysical model of UHECR sources to both the energy spectrum and mass composition data measured by the Pierre Auger Observatory. The fit has been performed for energies above 5.10(18) eV, i.e. the region of the all-particle spectrum above the so-called "ankle" feature. The astrophysical model we adopted consists of identical sources uniformly distributed in a comoving volume, where nuclei are accelerated through a rigidity-dependent mechanism. The fit results suggest sources characterized by relatively low maximum injection energies, hard spectra and heavy chemical composition. We also show that uncertainties about physical quantities relevant to UHECR propagation and shower development have a non-negligible impact on the fit results.

JOURNAL OF COSMOLOGY AND ASTROPARTICLE PHYSICS 4, 038, 2017. DOI: 10.1088/1475-7516/2017/04/038

[P133-2017] "Controlled stacking of graphene monolayer saturable absorbers for ultrashort pulse generation in erbium--doped fiber lasers"

Rosa, H. G.; **Castaneda, J. A.*; Brito Cruz, C. H.*; Padilha, L. A.*;** Gomes, J. C. V.; Thoroh de Souza, E. A.; **Fragnito, H. L.***

Stacked chemical-vapour deposited (CVD) graphene monolayer samples were fabricated and applied as saturable absorbers in erbium-doped fiber laser (EDFL). Transient absorption experiments show that at the saturation absorption regime, and regardless the number of stacked layers (from 1 to 5 layers), samples present 1 ps recovery time. Pulses with duration from 0.60 to 1.17 ps were generated in an EDFL, depending on the number of graphene layers (i.e., the linear optical absorption) used. The results show that it is possible to increase the linear optical absorption of a graphene stacking without affecting its nonlinear optical behavior and ultrafast response time. Therefore, by stacking individual CVD monolayer graphene samples it is possible to control the optical properties in graphene-based EDFLs and simultaneously tune their ultra-short pulse generation.

OPTICAL MATERIALS EXPRESS 7[7], 2528-2537, 2017. DOI: 10.1364/OME.7.002528

[P134-2017] "Crystallinity properties and crystallization behavior of chocolate fat blends"

da Silva, T. L. T.; Grimaldi, R.; **Calligaris, G. A.*; Cardoso, L. P.*;** Goncalves, L. A. G.

Cocoa butter (CB) provides unique crystallization characteristics to chocolates and confectionary products; hence, it is an important value-add product. However, other alternative fats that minimally affect the crystallization behaviour of chocolates and confectionary products are now being increasingly used. This study analyzed the crystallization behaviour of CB, cocoa butter substitutes (CBSs), and their blends. Blends were prepared using CBS concentrations: 5, 10, 15, 20 and 37.5%. CB, CBS, and their blends were evaluated by following analysis: solid fat content, isothermal analysis, polarized light microscopic, thermal behaviour, X-ray diffraction and consistency. Crystallization analysis showed an incompatibility between the 2 fats, with a reduction in the crystallinity and increase in liquid content in all the blends. Eutectic crystallization at 20 A degrees C was only observed for the blend containing 20% CBSs. This was considered as a positive result because previous studies have indicated that CBS concentration in CB blends should not be more than 5%.

JOURNAL OF FOOD SCIENCE AND TECHNOLOGY-MYSORE 54[7], 1979-1989, 2017. DOI: 10.1007/s13197-017-2634-4

[P135-2017] "Determination of Chlorophenol in Environmental Samples Using a Voltammetric Biosensor Based on Hybrid Nanocomposite"

Mendes, R. K.; Arruda, B. S.; de Souza, E. F.; Nogueira, A. B.; **Teschke, O.*; Bonugli, L. O.***; Etchegaray, A.

In this work, a simple electrochemical biosensor for 4-chlorophenol was developed based on laccase immobilized on a hybrid nanocomposite (ZnO nanoparticles/ chitosan), and incorporated in a carbon paste electrode. There are few biosensors in the literature for this specific pollutant because it tends to form polymeric films on the electrode, causing surface passivation or even enzyme inactivation. The carbon paste allowed the surface to be easily renewed by polishing, which amends this limitation. To optimize the experimental conditions, we used cyclic voltammetry and hydroquinone as a representative of phenolic compounds due to the high toxicity of chlorophenol, thus avoiding the generation of hazardous residues. After optimization, a calibration curve was constructed for 4-chlorophenol using differential pulse voltammetry, and a linear response was obtained from 1 to 50 mu M, with a lower detection limit of 0.7 mu M. The obtained biosensor showed high accuracy when employed in the analysis of industrial wastewater.

JOURNAL OF THE BRAZILIAN CHEMICAL SOCIETY 28[7], 1212-1219, 2017. DOI: 10.21577/0103-5053.20160282

[P136-2017] "Determination of the event collision time with the ALICE detector at the LHC"

Adam, J.; Adamova, D.; Aggarwal, M. M.; **Albuquerque, D. S. D.*; Chinellato, D. D.*; De Souza, R. D.*; Takahashi, J.***; et al. ALICE Collaboration

Particle identification is an important feature of the ALICE detector at the LHC. In particular, for particle identification via the time-of-flight technique, the precise determination of the event collision time represents an important ingredient of the quality of the measurement. In this paper, the different methods used for such a measurement in ALICE by means of the T0 and the TOF detectors are reviewed. Efficiencies, resolution and the improvement of the particle identification separation power of the methods used are presented for the different LHC colliding systems (pp, p-Pb and Pb-Pb) during the first period of data taking of LHC (Run 1).

EUROPEAN PHYSICAL JOURNAL PLUS 132[2], 99, 2017. DOI: 10.1140/epjp/i2017-11279-1

[P137-2017]"Direct measurement of clinical mammographic x-ray spectra using a CdTe spectrometer"

Santos, J. C.; **Tomal, A.***; Furquim, T. A.; Fausto, A. M. F.; Nogueira, M. S.; Costa, P. R.

Purpose: To introduce and evaluate a method developed for the direct measurement of mammographic x-ray spectra using a CdTe spectrometer. The assembly of a positioning system and the design of a simple and customized alignment device for this application is described. Methods: A positioning system was developed to easily and accurately locate the CdTe detector in the x-ray beam. Additionally, an alignment device to line up the detector with the central axis of the radiation beam was designed. Direct x-ray spectra measurements were performed in two different clinical mammography units and the measured x-ray spectra were compared with computer--generated spectra. In addition, the spectrometer misalignment effect was evaluated by comparing the measured spectra when this device is aligned relatively to when it is misaligned. Results: The positioning and alignment of the spectrometer have allowed the measurements of direct mammographic x-ray spectra in agreement with computer-generated spectra. The most accurate x-ray spectral shape, related with the minimal HVL value, and high photon fluence for measured spectra was found with the spectrometer aligned according to the proposed method. The HVL values derived from both simulated and measured x-ray spectra differ at most 1.3 and 4.5% for two mammography devices evaluated in this study. Conclusion: The experimental method developed in this work allows simple positioning and alignment of a spectrometer for x-ray spectra measurements given the geometrical constraints and maintenance of the original configurations of mammography machines.

MEDICAL PHYSICS 44[7], 3504-3511, 2017. DOI: 10.1002/mp.12287

[P138-2017] "Direct measurements of conventional and anisotropic magnetocaloric effect in binary RAl(2) single crystals"

Monteiro, J. C. B.*; Gandra, F. G.*

We report on specific heat and magnetocaloric effect (MCE) measurements in single crystals of HoAl2, DyAl2, and TbAl2 measured by a heat flux technique using Peltier devices. Those compounds order ferromagnetically at 31 K, 61 K, and 106 K respectively, and present a spin reorientation transition (SRT) below T-C. We study the dependence of the SRT with magnetic field and temperature by means of specific heat measurements performed in single crystals oriented at the [100], [110], and [111] directions with the aid of calculations using a simple model. We obtained the conventional MCE for HoAl2 and TbAl2 and also the anisotropic version of the effect obtained indirectly from the specific heat for TbAl2 and DyAl2. We also present the results for a direct determination of the anisotropic MCE for DyAl2 by measuring the heat flux generated by a rotation of the single crystal under constant field.

JOURNAL OF APPLIED PHYSICS 121[21], 213904, 2017. DOI: 10.1063/1.4984917

[P139-2017] "Doped tellurite glasses: Extending near-infrared emission for near-2.0-m amplifiers"

Seshadri, M.*; Anjos, V.; Bell, M. J. V.; **Barbosa, L. C.***; **Bosco, G. B. F.***; **Tessler, L. R.***; Kumar, J. S.; Graca, M. P. F.; Soares, M. J.; Radha, M.; Ratnakaram, Y. C.

Tm3+-singly-doped and Tm3+-/Ho3+-codoped TeO2-Bi2O3--ZnO-Li2O-Nb2O5 (TBZLN) tellurite glasses were successfully prepared by the melt-quenching technique. Emission characteristics and energy transfer mechanisms were studied upon 785-nm laser diode excitation. A significant enhancement of emission intensity at 1.81m with increasing concentration of Tm3+ ions has been observed while increase in the emission intensity at 2.0m with increasing concentration of Ho3+ has been observed up to the equal concentration of Tm3+ (0.5mol%) in TBZLN glasses. The stimulated emission cross section of Tm3+: (F4H6)-F-3-H-3 (5.20x10(-21)cm(2)) and Ho3+: (I7I8)-I-5-I-5 (4.00x10(-21)cm(2)) in 1.0mol% Tm3+-doped and 0.5mol% Tm3+/1.0mol% Ho3+-codoped TBZLN glasses are higher compared with the reported and are found to be excellent candidates for solid-state lasers operating at similar to 1.8 and 2.0m, respectively. The extension of near-infrared (NIR) emission of Tm3+ with Ho3+ ions provides the possibility of using these materials for broadband NIR amplifiers.

INTERNATIONAL JOURNAL OF APPLIED GLASS SCIENCE 8[2] SI, 216-225, 2017. DOI: 10.1111/ijag.12213

[P140-2017] "Encrypting Majorana fermion qubits as bound states in the continuum"

Guessi, L. H.; Dessotti, F. A.; Marques, Y.; Ricco, L. S.; Pereira, G. M.; **Menegasso, P.***; de Souza, M.; Seridonio, A. C.

We theoretically investigate a topological Kitaev chain connected to a double quantum-dot (QD) setup hybridized with metallic leads. In this system we observe the emergence of two striking phenomena: (i) a decrypted Majorana fermion (MF) qubit recorded over a single QD, which is detectable by means of conductance measurements due to the asymmetrical MF-qubit leaked state into the QDs; (ii) an encrypted qubit recorded in both QDs when the leakage is symmetrical. In such a regime, we have a cryptographylike manifestation, since the MF qubit becomes bound states in the continuum, which is not detectable in conductance experiments.

PHYSICAL REVIEW B 96[4], 041114, 2017. DOI: 10.1103/PhysRevB.96.041114

[P141-2017] "Energy dependence of forward-rapidity J/psi and psi (2S) production in pp collisions at the LHC"

Acharya, S.; Adamova, D.; **Albuquerque, D. S. D.*; Chinellato, D. D.*; De Souza, R. D.*; Takahashi, J.***; et al.
ALICE Collaboration

We present results on transverse momentum (p(T)) and rapidity (y) differential production cross sections, mean transverse momentum and mean transverse momentum square of inclusive J/psi and psi(2S) at forward rapidity (2.5 < y < 4) as well as psi(2S)--to-J/psi cross section ratios. These quantities are measured in pp collisions at center of mass energiesv root s = 5.02 and 13 TeV with the ALICE detector. Both charmonium states are reconstructed in the dimuon decay channel, using the muon spectrometer. Acomprehensive comparison to inclusive charmonium cross sections measured at root s = 2.76, 7 and 8 TeV is performed.

A comparison to non-relativistic quantum chromodynamics and fixed-order next-to-leading logarithm calculations, which describe prompt and non-prompt charmonium production respectively, is also presented. A good description of the data is obtained over the full p(T) range, provided that both contributions are summed. In particular, it is found that for p(T) > 15 GeV/c the non-prompt contribution reaches up to 50% of the total charmonium yield.

EUROPEAN PHYSICAL JOURNAL C 77[6], 392, 2017. DOI: 10.1140/epjc/s10052-017-4940-4

[P142-2017] "Evolution of the structural, energetic, and electronic properties of the 3d, 4d, and 5d transition-metal clusters (30 TMn systems for n=2-15): a density functional theory investigation"

Chaves, A. S.*; Piotrowski, M. J.; Da Silva, J. L. F.

Subnanometric transition-metal (TM) clusters have attracted great attention due to their unexpected physical and chemical properties, leastwise compared to their bulk counterparts. An in-depth understanding of the evolution of the properties as a function of the number of atoms for such systems is a basic prerequisite to leverage countless applications, from catalysis to magnetic storage, as well as to answer fundamental questions related to their intrinsic stability. Here, we reported a systematic density functional study to investigate the structural, electronic properties and stability of all TMn (30 elements) unary clusters as a function of the number of atoms (n = 2-15). We provided the complete structural patterns for all TM periodic table groups, considering the growth evolution as well as the main trends of the structural and electronic properties. The combination of the occupation of the bonding/anti-bonding d-states and the s-d hybridization is found to be the main stabilization mechanism, helping in the understanding of the structural patterns. Most TMn clusters have a magic number of atoms, for which there are peaks in s-d hybridization and null electric dipole moments. Thus, our extensive and comparative study addresses size effects along with the evolution of d-orbital occupation for the TMn gas-phase cluster properties.

PHYSICAL CHEMISTRY CHEMICAL PHYSICS 19[23], 15484-15502, 2017. DOI: 10.1039/c7cp02240a

[P143-2017] "Exploring from ab initio calculations the structural and electronic properties of supported metal linear atomic chains on the NiAl (110) surface"

Zornio, B. F.; **da Silva, E. Z.***; San-Miguel, M. A.

Periodic density functional theory calculations were carried out to study the energetic and electronic properties of group 10 and 11 transition metal linear atomic chains (LACs) supported on the NiAl (110) surface. The only crystallographic direction that produces an effective LAC is with the metal atoms along the [001] direction. In other directions, the atoms adsorbed on stable adsorption sites are separated by large distances reducing the metal-metal interactions and consequently, preventing the formation of chemical bonding. The growth process of adding atoms, one by one, in the effective LACs is energetically favorable by increasing the number of metal atoms, for all tested transition metals. The Pt LACs experience the strongest interaction between the metals within the LAC and the weakest interaction between the LAC and the support resulting in an outstanding behavior with respect to the other transition metals.

THEORETICAL CHEMISTRY ACCOUNTS 136[5], 63, 2017. DOI: 10.1007/s00214-017-2092-0

[P144-2017] "Fermi energy dependence of the optical emission in core/shell InAs nanowire homostructures"

Moller, M.*; Oliveira, D. S.*; Sahoo, P. K.*; Cotta, M. A.*; Iikawa, F.*; Motisuke, P.; Molina-Sanchez, A.; de Lima, M. M., Jr.; Garcia-Cristobal, A.; Cantarero, A.

InAs nanowires grown by vapor-liquid-solid (VLS) method are investigated by photoluminescence. We observe that the Fermi energy of all samples is reduced by similar to 20 meV when the size of the Au nanoparticle used for catalysis is increased from 5 to 20 nm. Additional capping with a thin InP shell enhances the optical emission and does not affect the Fermi energy. The unexpected behavior of the Fermi energy is attributed to the differences in the residual donor (likely carbon) incorporation in the axial (low) and lateral (high incorporation) growth in the VLS and vapor-solid (VS) methods, respectively. The different impurity incorporation rate in these two regions leads to a core/shell InAs homostructure. In this case, the minority carriers (holes) diffuse to the core due to the built-in electric field created by the radial impurity distribution. As a result, the optical emission is dominated by the core region rather than by the more heavily doped InAs shell. Thus, the photoluminescence spectra and the Fermi energy become sensitive to the core diameter. These results are corroborated by a theoretical model using a self-consistent method to calculate the radial carrier distribution and Fermi energy for distinct diameters of Au nanoparticles.

NANOTECHNOLOGY 28 [29], 295702, 2017. DOI: 10.1088/1361-6528/aa76bf

[P145-2017] "Gene flow and metacommunity arrangement affects coevolutionary dynamics at the mutualism - antagonism interface"

Lemos-Costa, P.; **Martins, A. B.***; Thompson, J. N.; **de Aguiar, M. A. M.***

Interspecific interactions are affected by community context and, as a consequence, show spatial variation in magnitude and sign. The selective forces imposed by interactions at the mutualism-antagonism interface are a consequence of the traits involved and their matching between species. If mutualistic and antagonistic communities are linked by gene flow, coevolution between a pair of interacting species is influenced by how selection varies in space. Here we investigate the effects of metacommunity arrangement, i.e. patterns of connection between communities and the number of communities, on the coevolutionary dynamics between two species for which the sign and magnitude of the interaction varies across the landscape. We quantify coevolutionary outcome as an index that can be decomposed into the contribution of intraspecific genetic diversity and interspecific interaction. We show that polymorphisms and mismatches are an expected outcome, which is influenced by spatial structure, interaction strength and the degree of gene flow. The index describes how variation is distributed within and between species, and provides information on the directionality of the mismatches and polymorphisms. Finally, we argue that depending on metacommunity arrangement, some communities have disproportionate roles in maintaining genetic diversity, with implications for the coevolution of interacting species in a fragmented landscape.

JOURNAL OF THE ROYAL SOCIETY INTERFACE 14[130], 20160989, 2017. DOI: 10.1098/rsif.2016.0989

[P146-2017] "High sensitivity thermal lens microscopy: Cr-VI trace detection in water"

Cedeno, E.; Cabrera, H.; Delgadillo-Lopez, A. E.; Delgado-Vasallo, O.; **Mansanares, A. M.***; Calderon, A.; Marin, E.

In this work, a low detection limit for hexavalent chromium in water of parts per trillions (21 ng/L) was achieved using a micro -spatial thermal lens spectroscopy setup with coaxial counter -propagating pump and probe laser beams and an integrated passive optical Fabry-Perot resonator, aided with a well -established diphenyl carbazide colorimetric method. Cr-VI concentrations in the range of mu g/L, i.e. well -below the toxicity thresholds in humans and animals (26 and 190 mg/L respectively) and below those delimited by international regulations for drink water (similar to 0.05-0.5 mg/L), have been obtained by measurements in bottled and tap water samples. The developed thermal lens microscope is also capable to detect Cr-VI directly in potassium dichromate solutions using pump beam wavelengths within the very low optical absorption region in the visible part of the spectrum, i.e., without the use of any calorimetric method.

TALANTA 170, 260-265, 2017. DOI: 10.1016/j.talanta.2017.04.008

[P147-2017] "Impact of the mobile terminal scheme on millimeter-wave radio over fiber systems based on photonic heterodyning techniques"

Aldaya, I.*; Campuzano, G.; Del-Valle-Soto, C.; Aragon-Zavala, A.; Castanon, G.

The use of communication networks relying on millimeter-wave (mm-wave) wireless links promises a great capacity enhancement as well as improved security. However, given the high-directivity of mm-wave links, coverage requirements are difficult to meet unless the network is assisted by an infrastructure. Given its low-cost, power-efficiency, and high capacity, radio over fiber has emerged as a strong candidate for the implementation of such infrastructure. Among the different generation techniques, photonic heterodyning has attracted considerable attention due to its capacity to generate radio frequency (RF) signals in the entire microwave/mm-wave range without requiring broadband electro-optical modulator. However, the RF signals generated using these techniques suffer from significant phase noise, a major impairment that degrades the system performance. In this paper we study two approaches to overcome this limitation: (1) the use of optical sideband injection locking (OSBIL) to generate tones with highly correlated phase noise and (2) heterodyning independent lasers in combination with a mobile terminal (MT) that is insensitive to the phase of the RF signal. A qualitative comparison between the two techniques in terms of MT sensitivity to the RF phase noise, the power sensitivity, and base station power efficiency leads to the conclusion that OSBIL is more suitable for networks with medium-range node separation, whereas heterodyning of independent laser with phase-insensitive MT is a cost-efficient solution for networks where nodes are closer to each other.

OPTICAL AND QUANTUM ELECTRONICS 49[6], 228, 2017. DOI: 10.1007/s11082-017-1058-8

[P148-2017] "Information Visualization and Feature Selection Methods Applied to Detect Gliadin in Gluten-Containing Foodstuff with a Microfluidic Electronic Tongue"

Daikuzono, C. M.; Shimizu, F. M.; Manzoli, A.; **Riul, A.***; Piazzetta, M. H. O.; Gobbi, A. L.; Correa, D. S.; Paulovich, F. V.; Oliveira, O. N.

The fast growth of celiac disease diagnosis has sparked the production of gluten-free food and the search for reliable methods to detect gluten in foodstuff. In this paper, we report on a microfluidic electronic tongue (e-tongue) capable of detecting trace amounts of gliadin, a protein of gluten, down to 0.005 mg kg(-1) in ethanol solutions, and distinguishing between gluten-free and gluten-containing foodstuff. In some cases, it is even possible to determine whether gluten-free foodstuff has been contaminated with gliadin. That was made possible with an e-tongue comprising four sensing units, three of which made of layer-by-layer (LbL) films of semiconducting polymers deposited onto gold interdigitated electrodes placed inside microchannels Impedance spectroscopy was employed as the principle of detection, and the electrical capacitance data collected with the e-tongue were treated with information visualization techniques with feature selection for optimizing performance. The sensing units are disposable to avoid cross-contamination as gliadin adsorbs irreversibly onto the LbL films according to polarization modulated infrared reflection absorption spectroscopy (PM-IRRAS) analysis. Small amounts of material are required to produce the nanostructured films, however, and the e--tongue methodology is promising for low-cost, reliable detection of gliadin and other gluten constituents in foodstuff.

ACS APPLIED MATERIALS & INTERFACES 9[23], 19646-19652, 2017. DOI: 10.1021/acsami.7b04252

[P149-2017] "Insights into the thermoelectric properties of SnSe from ab initio calculations"

Gonzalez-Romero, R. L.; **Antonelli, A.***; Melendez, J. J.

The thermoelectric properties of SnSe are studied by first-principles methods using an original methodology. We computed first the electronic structure of the system, which justifies its macroscopic anisotropy; the inclusion of van der Waals dispersive corrections improves the agreement of the structural parameters with experiments. The Seebeck coefficient and the electrical and thermal conductivities of single crystals and polycrystals are subsequently described in good agreement with experimental data. As for the electrical conductivity, values calculated with a temperature-dependent relaxation time compare well with the available measurements, especially for single crystals; in contrast, a constant relaxation time suffices to describe the results for polycrystals. Based on the iterative solution of the Boltzmann transport equation for phonons, we discuss the behavior of the thermal conductivity of the system in terms of its phonon spectrum. Finally, the figure of merit of SnSe single crystals and polycrystals is calculated and correlated with the previous discussions about electrical and thermal conductivities. From these findings, possible strategies to increase the figure of merit in practice are suggested.

PHYSICAL CHEMISTRY CHEMICAL PHYSICS 19[20], 12804-12815, 2017. DOI: 10.1039/c7cp01160a

[P150-2017] "Investigations of anharmonic effects via phonon mode variations in nanocrystalline Dy2O3, Gd2O3 and Y2O3"

Sharma, N. D.; Singh, J.; Vijay, A.; **Samanta, K.***; Pandey, S. D.

The nanocrystalline rare earth sesquioxides Dy2O3, Gd2O3 and Y2O3 have been investigated for anharmonic effects in the temperature range 80-440K using Raman spectroscopy. These samples were cubic in structure under ambient conditions with particle sizes in nano-range. The predominant T-g+A(g) phonon modes of the samples primarily exhibited phonon softening in the investigated temperature range. However, the line width variations clearly reflected the variations in the effects of anharmonicity on these samples, and the related anharmonic constants were estimated. The mode Grueneisen parameters required for these studies were deduced from our own high-pressure data for these samples reported earlier. The line width variations for these samples were found to display similar trends; however, their magnitudes were indicative of the factors that are expected to contribute to the variation in phonon behaviour.

JOURNAL OF RAMAN SPECTROSCOPY 48[6], 822-828, 2017. DOI: 10.1002/jrs.5120

[P151-2017] "K*(892)(0) and phi(1020)meson production at high transverse momentum in pp and Pb-Pb collisions at root sNN=2.76 TeV"

Adam, J.; Adamova, D.; Aggarwal, M. M.; **Albuquerque, D. S. D.*; Chinellato, D. D.*; De Souza, R. D.*; Takahashi, J.***; et al.
ALICE Collaboration

The production of K*(892)(0) and phi(1020) mesons in proton--proton (pp) and lead-lead (Pb-Pb) collisions at root sNN = 2.76 TeV has been analyzed using a high luminosity data sample accumulated in 2011 with the ALICE detector at the Large Hadron Collider (LHC). Transverse momentum (p(T)) spectra have been measured for K*(892)(0) and phi(1020) mesons via their hadronic decay channels for p(T) up to 20 GeV/c. The measurements in pp collisions have been compared to model calculations and used to determine the nuclear modification factor and particle ratios. The K*(892)(0)/K ratio exhibits significant reduction from pp to central Pb-Pb collisions, consistent with the suppression of the K*(892)(0) yield at low pT due to rescattering of its decay products in the hadronic phase. In central Pb-Pb collisions the pT dependent phi(1020)/p and K*(892)0/p ratios show an enhancement over pp collisions for pT approximate to 3 GeV/c, consistent with previous observations of strong radial flow. At high pT, particle ratios in Pb-Pb collisions are similar to those measured in pp collisions. In central Pb-Pb collisions, the production of K*(892)(0) and phi(1020) mesons is suppressed for p(T) > 8 GeV/c. This suppression is similar to that of charged pions, kaons, and protons, indicating that the suppression does not depend on particle mass or flavor in the light quark sector.

PHYSICAL REVIEW C 95[6], 064606, 2017. DOI: 10.1103/PhysRevC.95.064606

[P152-2017] "Long-time efficacy of the surface code in the presence of a super-Ohmic environment"

Lopez-Delgado, D. A.*; Novais, E.; Mucciolo, E. R.; **Caldeira, A. O.***

We study the long-time evolution of a quantum memory coupled to a bosonic environment on which quantum error correction (QEC) is performed using the surface code. The memory's evolution encompasses N QEC cycles, each of them yielding a nonerror syndrome. This assumption makes our analysis independent of the recovery process. We map the expression for the time evolution of the memory onto the partition function of an equivalent statistical-mechanical spin system. In the super-Ohmic dissipation case the long-time evolution of the memory has the same behavior as the time evolution for just one QEC cycle. For this case we find analytical expressions for the critical parameters of the order-disorder phase transition of an equivalent spin system. These critical parameters determine the threshold value for the system-environment coupling below which it is possible to preserve the memory's state.

PHYSICAL REVIEW A 95[6], 062328, 2017. DOI: 10.1103/PhysRevA.95.062328

[P153-2017] "Low-temperature Raman spectra of the 2-(alpha-methylbenzylamino)-5-nitropyridine crystal"

Pinheiro, G. S.; Ferreira Junior, M. N. G.; dos Santos, A. O.; Freire, P. T. C.; Lima, J. A.; Nogueira, C. E. S.; **Cardoso, L. P.***; Sherwood, J. N.; Remedios, C. M. R.

The polar organic 2-(alpha-methylbenzylamino)-5-nitropyridine crystal (MBANP) has been studied by Raman spectroscopy at low temperatures (from 300 to 10 K). The effect of temperature change on the vibrational spectrum is discussed with the aid of DFT calculations. The behavior of the Raman spectra indicates that MBANP molecules present a different conformation at low temperatures associated with the rotation of the phenyl and pyridine rings. Temperature -dependent X-ray measurements and differential scanning calorimetry (DSC) analysis were utilized as complementary techniques to investigate the structural stability of MBANP crystal.

SPECTROCHIMICA ACTA PART A-MOLECULAR AND BIOMOLECULAR SPECTROSCOPY 183, 209-217, 2017. DOI: 10.1016/j.saa.2017.04.055

[P154-2017] "Magnetocaloric effect investigation in the ferromagnetic Eu2CuSi3 compound"

Silva, M. G.; **de Paula, V. G.***; dos Santos, A. O.; **Coelho, A. A.*; Cardoso, L. P.***; da Silva, L. M.

Here, it is reported the study of the structural, magnetic properties and magnetocaloric effect (MCE) of the Eu2CuSi3 compound. Polycrystalline Eu2CuSi3 compound with AlB2-type derived hexagonal structure was successfully synthesized by arc-melting method. Magnetic measurements indicate a second-order ferromagnetic (FM) phase transition below 40 K. The effective magnetic moment of Eu is reduced compared with divalent free ion, indicating a compensation of Eu magnetic moment. Spin reorientation induce negative magnetocaloric effect below Curie temperature. The values of full width half-maximum of -Delta S-M peak (delta T-FWHM = 35 K) and maximum value of entropy change (- Delta S-M(Mix) similar to 9.5 J/kg K) for mu(0)Delta H = 6 T strongly contribute to improve the relative cooling power (RCP similar to 332 J/kg) of Eu2CuSi3 compound. As observed, delta T-FWHM value is sensibly wider than the usual values observed for first and second order magnetic phase transition compounds. Then, - Delta S-M(max) and delta T-FWHM values as well as the neglected magnetic hysteresis that were obtained for Eu2CuSi3 have shown features as a desirable second order magnetic phase transition compound for low temperature magnetic refrigeration.

INTERMETALLICS 88, 36-40, 2017. DOI: 10.1016/j.intermet.2017.04.013

[P155-2017] "Measurement of electroweak-induced production of W gamma with two jets in pp collisions at root s=8TeV and constraints on anomalous quartic gauge couplings"

Khachatryan, V.; Sirunyan, A. M.; Tumasyan, A.; **Chinellato, J. A.*; Tonelli Manganote, E. J.***; et al.
CMS Collaboration

A measurement of electroweak-induced production of W gamma and two jets is performed, where the W boson decays leptonically. The data used in the analysis correspond to an integrated luminosity of 19.7 fb(-1) collected by the CMS experiment in root s = 8TeV proton-proton collisions produced at the LHC. Candidate events are selected with exactly one muon or electron, missing transverse momentum, one photon, and two jets with large rapidity separation. An excess over the hypothesis of the standard model without electroweak production of W gamma with two jets is observed with a signi fi cance of 2.7 standard deviations. The cross section measured in the fi ducial region is 10.8 +/- 4.1(stat) +/- 3.4(syst) +/- 0. 3(lumi) fb, which is consistent with the standard model electroweak prediction. The total cross section for W gamma in association with two jets in the same fi ducial region is measured to be 23.2 +/- 4.3(stat) +/- 1.7(syst) +/- 0.6(lumi) fb, which is consistent with the standard model prediction from the combination of electroweakand quantum chromodynamics-induced processes. No deviations are observed from the standard model predictions and experimental limits on anomalous quartic gauge couplings integral M,0- 7 /Lambda(4), integral T,0- 2 /Lambda(4), and integral T,5-7/Lambda(4) are set at 95% con fi dence level.

JOURNAL OF HIGH ENERGY PHYSICS 6, 106, 2017. DOI: 10.1007/JHEP06(2017)106

[P156-2017] "Measurement of the cross section for electroweak production of Z gamma in association with two jets and constraints on anomalous quartic gauge couplings in proton-proton collisions at root s=8 TeV"

Khachatryan, V.; Sirunyan, A. M.; Tumasyan, A.; **Chinellato, J. A.*; Tonelli Manganote, E. J.*;** et al.
CMS Collaboration

A measurement is presented of the cross section for the electroweak production of a Z boson and a photon in association with two jets in proton-proton collisions at root s = 8 TeV. The Z bosons are identified through their decays to electron or muon pairs. The measurement is based on data collected with the CMS detector corresponding to an integrated luminosity of 19.7 fb(-1). The electroweak contribution has a significance of 3.0 standard deviations, and the measured fiducial cross section is 1.86(-0.75)(+0.90)(stat)(-0.26)(+0.34)(syst) +/- 0.05(lumi) fb, while the summed electroweak and quantum chromodynamic total cross section in the same region is observed to be 5.94(-1.35)(+1.53) (stat)(-0.37)(+0.43)(syst) +/- 0.13(lumi) fb. Both measurements are consistent with the leading-order standard model predictions. Limits on anomalous quartic gauge couplings are set based on the Z gamma mass distribution.

PHYSICS LETTERS B 770, 380-402, 2017. DOI: 10.1016/j.physletb.2017.04.071

[P157-2017] "Measurement of the mass difference between top quark and antiquark in pp collisions at root s=8 TeV"

Chatrchyan, S.; Khachatryan, V.; Sirunyan, A. M.; **Chinellato, J. A.*; Tonelli Manganote, E. J.*;** et al.
CMS Collaboration

The invariance of the standard model (SM) under the CPT transformation predicts equality of particle and antiparticle masses. This prediction is tested by measuring the mass difference between the top quark and antiquark (Delta m(t) = m(t) - m((t) over bar)) that are produced in pp collisions at a center-of-mass energy of 8 TeV, using events with a muon or an electron and at least four jets in the final state. The analysis is based on data corresponding to an integrated luminosity of 19.6 fb(-1) collected by the CMS experiment at the LHC, and yields a value of Delta m(t) = 0.15 0.19 (stat) +/- 0.09(syst) GeV, which is consistent with the SM expectation. This result is significantly more precise than previously reported measurements.

PHYSICS LETTERS B 770, 50-71, 2017. DOI: 10.1016/j.physletb.2017.04.028

[P158-2017] "Measurement of the top quark mass using single top quark events in proton-proton collisions at root s=8 TeV"

Sirunyan, A. M.; Tumasyan, A.; Adam, W.; **Chinellato, J. A.*; Tonelli Manganote, E. J.***; et al.
CMS Collaboration

A measurement of the top quark mass is reported in events containing a single top quark produced via the electroweak t channel. The analysis is performed using data from proton--proton collisions collected with the CMS detector at the LHC at a centre-of-mass energy of 8 TeV, corresponding to an integrated luminosity of 19.7 fb(-1). Top quark candidates are reconstructed from their decay to a W boson and a b quark, with the W boson decaying leptonically to a muon and a neutrino. The final state signature and kinematic properties of single top quark events in the t channel are used to enhance the purity of the sample, suppressing the contribution from top quark pair production. A fit to the invariant mass distribution of reconstructed top quark candidates yields a value of the top quark mass of 172.95 +/- 0.77 (stat)(-0.93)(+0.97) (syst) GeV. This result is in agreement with the current world average, and represents the first measurement of the top quark mass in event topologies not dominated by top quark pair production, therefore contributing to future averages with partially uncorrelated systematic uncertainties and a largely uncorrelated statistical uncertainty.

EUROPEAN PHYSICAL JOURNAL C 77[5], 354, 2017. DOI: 10.1140/epjc/s10052-017-4912-8

[P159-2017] "Mechanical properties and fracture patterns of graphene (graphitic) nanowiggles"

Bizao, R. A.*; Botari, T.*; Perim, E.; Pugno, Nicola M.; **Galvao, D. S.***

Graphene nanowiggles (GNW) are graphene-based nanostructures obtained by making alternated regular cuts in pristine graphene nanoribbons. GNW were recently synthesized and it was demonstrated that they exhibit tunable electronic and magnetic properties by just varying their shape. Here, we have investigated the mechanical properties and fracture patterns of a large number of GNW of different shapes and sizes using fully atomistic reactive molecular dynamics simulations. Our results show that the GNW mechanical properties are strongly dependent on its shape and size and, as a general trend narrow sheets have larger ultimate strength and Young's modulus than wide ones. The estimated Young's modulus values were found to be in a range of approximate to 100 - 1000 GPa and the ultimate strength in a range of approximate to 20 - 110 GPa, depending on GNW shape. Also, super-ductile behavior under strain was observed for some structures.

CARBON 119, 431-437, 2017. DOI: 10.1016/j.carbon.2017.04.018

[P160-2017]" Microfluidic Electronic Tongue Applied to Soil Analysis"

Braunger, M. L.*; Shimizu, F. M.; **Jimenez, M. J. M.***; Amaral, L. R.; Piazzetta, M. H. O.; Gobbi, A. L.; Magalhaes, P. S. G.; **Rodrigues, V.***; Oliveira, O. N.; **Riul, A.***

Precision agriculture is crucial for increasing food output without expanding the cultivable area, which requires sensors to be deployed for controlling the level of nutrients in the soil. In this paper, we report on a microfluidic electronic tongue (e-tongue) based on impedance measurements which is capable of distinguishing soil samples enriched with plant macronutrients. The e-tongue setup consisted of an array of sensing units made with layer-by-layer films deposited onto gold interdigitated electrodes. Significantly, the sensing units could be reused with adequate reproducibility after a simple washing procedure, thus indicating that there is no cross--contamination in three independent sets of measurements. A high performance was achieved by treating the capacitance data with the multidimensional projection techniques Principal Component Analysis (PCA), Interactive Document Map (IDMAP), and Sammon's Mapping. While an optimized performance was demonstrated with IDMAP and feature selection, during which data of a limited frequency range were used, the distinction of all soil samples was also possible with the well-established PCA analysis for measurements at a single frequency. The successful use of a simple microfluidic e-tongue for soil analysis paves the way for enhanced tools to support precision agriculture.

CHEMOSENSORS 5[2], 14, 2017. DOI: 10.3390/chemosensors5020014

[P161-2017] "Molecular Dynamics of H-2 Storage in Carbon Nanotubes Under External Electric Field Effects: A Sensor Proposal"

Aires, J. C. N.; Neto, A. F. G.; Maneschy, C. E.; Huda, M. N.; Anjos, A. R.; **Riul, A.***; Souza, J. F.; Neto, A. M. J. C.

We present an analysis on molecular dynamics between H-2 molecule interacting with one carbon nanotube section at low initial-temperature of simulation, corresponding to 10(-3) K, and under constant electric field effects, in order to verify the performance of the carbon nanotube like a H-2 sensor, and consequently, indicating its use as an effective internal coating in storage tanks of hydrogen gas. During simulations, the H-2 was relaxed for 40 ps inside and outside of carbon nanotube, describing each possible arrangement for the capture of H-2, and electric field was applied over the system, longitudinally to the carbon nanotube length, promoting the rise of an evanescent field, able to trap H-2, which orbited the carbon nanotube. Simulations for electric fields intensities in a range of 10(-8) au up to 10(-6) au were performed, and mean orbit radius are estimated, as well as, some physical quantities of the system. The quantities calculated were: kinetic energy, potential energy, total energy and temperature in situ, among molar entropy variation. Our results indicates that a combination of electric field and van der Walls interactions derivatives of carbon nanotube is enough to create an evanescent field with attractive potential, showing it system as a good H-2 sensor.

JOURNAL OF NANOSCIENCE AND NANOTECHNOLOGY 17[7], 4858-4863, 2017. DOI: 10.1166/jnn.2017.13446

[P162-2017] "Multi-resolution anisotropy studies of ultrahigh-energy cosmic rays detected at the Pierre Auger Observatory"

Aab, A.; Abreu, P.; Aglietta, M.; **Chinellato, J. A.*; Daniel, B.*; Diaz Castro, M. L.*; Dobrigkeit, C.*; Escobar, C. O.*; Fauth, A. C.*; Kemp, E.*; Muller, M. A.*; Pakk Selmi-Dei, D.*; Pereira, L. A. S.*; Theodoro, V. M.***; et al.
Pierre Auger Collaboration

We report a multi-resolution search for anisotropies in the arrival directions of cosmic rays detected at the Pierre Auger Observatory with local zenith angles up to 80 degrees and energies in excess of 4EeV (4 x 10(18) eV). This search is conducted by measuring the angular power spectrum and performing a needlet wavelet analysis in two independent energy ranges. Both analyses are complementary since the angular power spectrum achieves a better performance in identifying large-scale patterns while the needlet wavelet analysis, considering the parameters used in this work, presents a higher efficiency in detecting smaller-scale anisotropies, potentially providing directional information on any observed anisotropies. No deviation from isotropy is observed on any angular scale in the energy range between 4 and 8EeV. Above 8EeV, an indication for a dipole moment is captured; while no other deviation from isotropy is observed for moments beyond the dipole one. The corresponding p-values obtained after accounting for searches blindly performed at several angular scales, are 1.3 x 10(-5) in the case of the angular power spectrum, and 2.5 x 10(-3) in the case of the needlet analysis. While these results are consistent with previous reports making use of the same data set, they provide extensions of the previous works through the thorough scans of the angular scales.

JOURNAL OF COSMOLOGY AND ASTROPARTICLE PHYSICS 6, 026, 2017. DOI: 10.1088/1475-7516/2017/06/026

[P163-2017] "Neutrino oscillations from warped flavor symmetry: Predictions for long baseline experiments T2K, NOvA, and DUNE"

Pasquini, P.*; Chulia, S. C.; Valle, J. W. F.

Here we study the pattern of neutrino oscillations emerging from a previously proposed warped standard model construction incorporating Delta(27) flavor symmetry [J. High Energy Phys. 01 (2016) 007]. In addition to a complete description of fermion masses, the model predicts the lepton mixing matrix in terms of two parameters. The good measurement of. theta(13) makes these two parameters tightly correlated, leading to an approximate one-parameter description of neutrino oscillations. We find secondary minima for the CP phase absent in the general unconstrained oscillation scenario and determine the fourfold degenerate sharp correlation between the physical CP phase delta(CP) and the atmospheric mixing angle. theta(23). This implies that maximal. theta(23) correlates with maximal leptonic CP violation. We perform a realistic estimate of the total neutrino and antineutrino event numbers expected at long baseline oscillation experiments T2K, NOvA, and the upcoming DUNE proposal. We show how an improved knowledge of the CP phase will probe the model in a significant way.

PHYSICAL REVIEW D 95[9], 095030, 2017. DOI: 10.1103/PhysRevD.95.095030

[P164-2017] "On the phonon dissipation contribution to nanoscale friction by direct contact"

de Mello, S. R. S.; da Costa, M. E. H. M.; Menezes, C. M.; Boeira, C. D.; Freire, F. L., Jr.; **Alvarez, F.***; Figueroa, C. A.

The friction phenomenon is a ubiquitous manifestation of nature. Models considering phononic, electronic, magnetic, and electrostatic interactions are invoked to explain the fundamental forces involved in the friction phenomenon. In order to establish the incidence of the phonon prompting at the nanoscale friction by direct contact, we study a diamond spherical dome sliding on carbon thin films containing different amount of deuterium and hydrogen. The friction coefficient decreases by substituting hydrogen by deuterium atoms. This result is consistent with an energy dissipation vibration local mechanism from a disordered distribution of bond terminators.

SCIENTIFIC REPORTS 7, 3242, 2017. DOI: 10.1038/s41598-017-03046-8

[P165-2017] "Parameter limits for neutrino oscillation with decoherence in KamLAND"

Gomes, G. B.*; Guzzo, M. M.*; de Holanda, P. C.*; Oliveira, R. L. N.*

In the framework of open quantum systems, we analyze data from KamLAND by using a model that considers neutrino oscillation in a three-family approximation with the inclusion of the decoherence effect. Using chi(2) test, we find new limits for the decoherence parameter, which we call gamma, considering the most recent data by KamLAND. Assuming an energy dependence of the type gamma=gamma(0) (E/E-0)(n), at a 95% C.L., the limits found are 3.7 x 10(-24) GeV for n=-1, 6.8 x 10(-22) GeV for n=0, and 1.5 x 10(-19) GeV for n=1 on the energy dependence.

PHYSICAL REVIEW D 95[11], 113005, 2017. DOI: 10.1103/PhysRevD.95.113005

[P166-2017] "Production of muons from heavy-flavour hadron decays in p-Pb collisions at root s(NN)=5.02 TeV"

Acharya, S.; Adamova, D.; Aggarwal, M. M.; **Albuquerque, D. S. D.*; Chinellato, D. D.*; De Souza, R. D.*; Takahashi, J.***; et al.
ALICE Collaboration

The production of muons from heavy-flavour hadron decays in p-Pb collisions at root s(NN) = 5.02 TeV was studied for 2 < p(T) < 16 GeV/c with the ALICE detector at the CERN LHC. The measurement was performed at forward (p-going direction) and backward (Pb-going direction) rapidity, in the ranges of rapidity in the centre-of-mass system (cms) 2.03 < y(cms) < 3.53 and -4.46 < y(cms) < -2.96, respectively. The production cross sections and nuclear modification factors are presented as a function of transverse momentum (P-T). At forward rapidity, the nuclear modification factor is compatible with unity while at backward rapidity, in the interval 2.5 < p(T) < 3.5 GeV/c, it is above unity by more than 2 sigma. The ratio of the forward -to -backward production cross sections is also measured in the overlapping interval 2.96 < |y(cms)| < 3.53 and is smaller than unity by 3.7 sigma in 2.5 < p(T) < 3.5 GeV/c. The data are described by model calculations including cold nuclear matter effects.

PHYSICS LETTERS B 770, 459-472, 2017. DOI: 10.1016/j.physletb.2017.03.049

[P167-2017] "Production of Sigma(1385)(+/-) and Xi(1530)(0) in p-Pb collisions at root s(NN)=5.02 TeV"

Adamova, D.; Aggarwal, M. M.; **Albuquerque, D. S. D.*; Chinellato, D. D.*; De Souza, R. D.*; Takahashi, J.***; et al.
ALICE Collaboration

The transverse momentum distributions of the strange and double-strange hyperon resonances (Sigma (1385)(+/-), Xi (1530)(0)) produced in p-Pb collisions at root s(NN) = 5.02 TeV were measured in the rapidity range -0.5 < yCMS < 0 for event classes corresponding to different charged-particle multiplicity densities, < dN(ch)/d eta(lab)> . The mean transverse momentumvalues are presented as a function of < dNch/d eta(lab)>, as well as a function of the particle masses and compared with previous results on hyperon production. The integrated yield ratios of excited to ground- state hyperons are constant as a function of < dN(ch)/d eta(lab)>. The equivalent ratios to pions exhibit an increase with < dN(ch)/ d eta(lab)>, depending on their strangeness content.

EUROPEAN PHYSICAL JOURNAL C 77[6], 389, 2017. DOI: 10.1140/epjc/s10052-017-4943-1

[P168-2017]" SAMPA Chip: the New 32 Channels ASIC for the ALICE TPC and MCH Upgrades"

Adolfsson, J.; Ayala Pabon, A.; Bregant, M.; Britton, C.; Brulin, G.; Carvalho, D.; Chambert, V.; **Chinellato, D. D.*;** Espagnon, B.; Hernandez Herrera, H. D.; Ljubicic, T.; Mahmood, S. M.; Mjornmark, U.; Moraes, D.; Munhoz, M. G.; Noel, G.; Oskarsson, A.; Osterman, L.; Pilyar, A.; Read, K.; **Ruette, A.*;** Russo, P.; Sanches, B. C. S.; Severo, L.; Silvermyr, D.; Suire, C.; Tambave, G. J.; Tun-Lanoe, K. M. M.; van Noije, W.; Velure, A.; Vereschagin, S.; Wanlin, E.; Weber, T. O.; Zaporozhets, S.

This paper presents the test results of the second prototype of SAMPA, the ASIC designed for the upgrade of read-out front end electronics of the ALICE Time Projection Chamber (TPC) and Muon Chamber (MCH). SAMPA is made in a 130 nm CMOS technology with 1.25V nominal voltage supply and provides 32 channels, with selectable input polarity, and three possible combinations of shaping time and sensitivity. Each channel consists of a Charge Sensitive Amplifier, a semi-Gaussian shaper and a 10-bit ADC; a Digital Signal Processor provides digital filtering and compression capability. In the second prototype run both full chip and single test blocks were fabricated, allowing block characterization and full system behaviour studies. Experimental results are here presented showing agreement with requirements for both the blocks and the full chip.

JOURNAL OF INSTRUMENTATION 12, C04008, 2017. DOI: 10.1088/1748-0221/12/04/C04008

[P169-2017] "Search for dijet resonances in proton-proton collisions at root s=13 TeV and constraints on dark matter and other models"

Sirunyan, A. M.; Tumasyan, A.; Adam, W.; **Chinellato, J. A.*; Tonelli Manganote, E. J.***; et al.
CMS Collaboration

A search is presented for narrow resonances decaying to dijet final states in proton-proton collisions at root s = 13 TeV using data corresponding to an integrated luminosity of 12.9 fb(-1). The dijet mass spectrum is well described by a smooth parameterization and no significant evidence for the production of new particles is observed. Upper limits at 95% confidence level are reported on the production cross section for narrow resonances with masses above 0.6TeV. In the context of specific models, the limits exclude string resonances with masses below 7.4TeV, scalar diquarks below 6.9TeV, axigluons and colorons below 5.5TeV, excited quarks below 5.4TeV, color-octet scalars below 3.OTeV, W' bosons below 2.7 TeV, Z' bosons below 2.1 TeV and between 2.3 and 2.6 TeV, and RS gravitons below 1.9 TeV. These extend previous limits in the dijet channel. Vector and axial--vector mediators in a simplified model of interactions between quarks and dark matter are excluded below 2.0 TeV. The first limits in the dijet channel on dark matter mediators are presented as functions of dark matter mass and are compared to the exclusions of dark matter in direct detection experiments.

PHYSICS LETTERS B 769, 520-542, 2017. DOI: 10.1016/j.physletb.2017.02.012

[P170-2017] "Search for heavy gauge W ' bosons in events with an energetic lepton and large missing transverse momentum at root s=13TeV"

Khachatryan, V.; Sirunyan, A. M.; Tumasyan, A.; **Chinellato, J. A.*; Tonelli Manganote, E. J.*;** et al.
CMS Collaboration

A search is presented for W' bosons in events with an electron or muon and large missing transverse momentum, using proton-proton collision data at root s = 13 TeV collected with the CMS detector in 2015 and corresponding to an integrated luminosity of 2.3 fb(-1). No evidence of an excess of events relative to the standard model expectations is observed. For a W' boson described by the sequential standard model, upper limits at 95% confidence level are set on the product of the production cross section and branching fraction and lower limits are established on the new boson mass. Masses below 4.1 TeV are excluded combining electron and muon decay channels, significantly improving upon the results obtained with the 8 TeV data. Exclusion limits at 95% confidence level on the product of the W' production cross section and branching fraction are also derived in combination with the 8 TeV data. Finally, exclusion limits are set for the production of generic W' bosons decaying into this final state using a model-independent approach.

PHYSICS LETTERS B 770, 278-301, 2017. DOI: 10.1016/j.physletb.2017.04.043

[P171-2017] "Search for photons with energies above 10(18) eV using the hybrid detector of the Pierre Auger Observatory"

Aab, A.; Abreu, P.; Aglietta, M.; **Chinellato, J. A.*; Daniel, B.*; Diaz Castro, M. L.*; Dobrigkeit, C.*; Fauth, A. C.*; Kemp, E.*; Muller, M. A.*; Pereira, L. A. S.*; Theodoro, V. M.*;** et al.
Pierre Auger Collaboration

A search for ultra-high energy photons with energies above 1 EeV is performed using nine years of data collected by the Pierre Auger Observatory in hybrid operation mode.

An unprecedented separation power between photon and hadron primaries is achieved by combining measurements of the longitudinal air-shower development with the particle content at ground measured by the fluorescence and surface detectors, respectively. Only three photon candidates at energies 1{2 EeV are found, which is compatible with the expected hadron-induced background. Upper limits on the integral flux of ultra-high energy photons of 0.027, 0.009, 0.008, 0.008 and 0.007 km(-2) sr(-1) yr(-1) are derived at 95% C.L. for energy thresholds of 1, 2, 3, 5 and 10 EeV. These limits bound the fractions of photons in the all-particle integral flux below 0.1%, 0.15%, 0.33%, 0.85% and 2.7%. For the first time the photon fraction at EeV energies is constrained at the sub-percent level. The improved limits are below the flux of diffuse photons predicted by some astrophysical scenarios for cosmogenic photon production. The new results rule-out the early top-down models in which ultra-high energy cosmic rays are produced by, e.g., the decay of super-massive particles and challenge the most recent super-heavy dark matter models.

JOURNAL OF COSMOLOGY AND ASTROPARTICLE PHYSICS 4, 009, 2017. DOI: 10.1088/1475-7516/2017/04/009

[P172-2017] "Search for single productio no vector-like quarks decaying to a Z boson and a top or a bottom quark in proton-proton collisions at root s=13 TeV"

Sirunyan, A. M.; Tumasyan, A.; Adam, W.; **Chinellato, J. A.*; Tonelli Manganote, E. J.*;** et al.
CMS Collaboration

A search for single production of vector-like quarks, T and B, decaying into a Z boson and a top or a bottom quark, respectively, is presented. The search is performed using data collected by the CMS experiment at the LHC in proton-proton collisions at root s = 13TeV, corresponding to an integrated luminosity of 2.3 fb(-1). An exotic T quark production mode through the decay of a heavy Z' resonance is also considered. The search is performed in events with a Z boson decaying leptonically, accompanied by a bottom or a top quark decaying hadronically. No excess of events is observed over the standard model background expectation. Products of production cross section and branching fraction for T and B quarks from 1.26 and 0.13 pb are excluded at 95% confidence level for the range of resonance mass considered, which is between 0.7 and 1.7TeV. Limits on the product of the Z 0 boson production cross section and branching fraction, with the Z' boson decaying to the Tt final state, are set between 0.31 and 0.13 pb, for Z' boson masses in the range from 1.5 to 2.5 TeV. This is the first search at 13TeV for single production of vector-like quarks in events with a Z boson decaying leptonically accompanied by boosted jets.

JOURNAL OF HIGH ENERGY PHYSICS 5, 029, 2017. DOI: 10.1007/JHEP05(2017)029

[P173-2017] "Search for supersymmetry in events with photons and missing transverse energy in pp collisions at 13 TeV"

Khachatryan, V.; Sirunyan, A. M.; Tumasyan, A.; **Chinellato, J. A.*; Tonelli Manganote, E. J.***; et al.
CMS Collaboration

The results of a search for new physics in final states with photons and missing transverse energy are reported. The study is based on a sample of proton-proton collisions collected at a center-of-mass energy of 13 TeV with the CMS detector in 2015, corresponding to an integrated luminosity of 2.3 fb(-1). Final states with two photons and significant missing transverse energy are used to search for supersymmetric particles in models of supersymmetry (SUSY) with general gauge-mediated (GGM) supersymmetry breaking. No excess is observed with respect to the standard model expectation, and the results are used to set limits on gluino pair production and squark pair production in the GGM SUSY framework. Gluino masses below 1.65 TeV and squark masses below 1.37 TeV are excluded at a 95% confidence level.

PHYSICS LETTERS B 769, 391-412, 2017. DOI: 10.1016/j.physletb.2017.04.005

[P174-2017] "Search for t(t)over-bar resonances in highly boosted lepton plus jets and fully hadronic final states in proton-proton collisions at root s=13 TeV"

Sirunyan, A. M.; Tumasyan, A.; Adam, W.; **Chinellato, J. A.*; Tonelli Manganote, B.***; et al.
CMS Collaboration

A search for the production of heavy resonances decaying into top quark-antiquark pairs is presented. The analysis is performed in the lepton+jets and fully hadronic channels using data collected in proton-proton collisions at root s = 13 TeV using the CMS detector at the LHC, corresponding to an integrated luminosity of 2.6 fb(-1). The selection is optimized for massive resonances, where the top quarks have large Lorentz boosts. No evidence for resonant t (t) over bar production is found in the data, and upper limits on the production cross section of heavy resonances are set. The exclusion limits for resonances with masses above 2 TeV are significantly improved compared to those of previous analyses at root s = 8 TeV.

JOURNAL OF HIGH ENERGY PHYSICS 7, 001, 2017. DOI: 10.1007/JHEP07(2017)001

[P175-2017] "Searches for pair production of third-generation squarks in root s=13 TeV pp collisions"

Sirunyan, A. M.; Tumasyan, A.; Adam, W.; **Chinellato, J. A.*; Tonelli Manganote, E. J.***; et al.
CMS Collaboration

Searches are presented for direct production of top or bottom squark pairs in proton-proton collisions at the CERN LHC. Two searches, based on complementary techniques, are performed in all-jet final states that are characterized by a significant imbalance in transverse momentum. An additional search requires the presence of a charged lepton isolated from other activity in the event. The data were collected in 2015 at a centre-of-mass energy of 13 TeV with the CMS detector and correspond to an integrated luminosity of 2.3 fb(-1). No statistically significant excess of events is found beyond the expected contribution from standard model processes. Exclusion limits are set in the context of simplified models of top or bottom squark pair production. Models with top and bottom squark masses up to 830 and 890 GeV, respectively, are probed for light neutralinos. For models with top squark masses of 675 GeV, neutralino masses up to 260 GeV are excluded at 95% confidence level.

EUROPEAN PHYSICAL JOURNAL C 77[5], 327, 2017. DOI: 10.1140/epjc/s10052-017-4853-2

[P176-2017] "Simplifying the design of microstructured optical fibre pressure sensors"

Osorio, J. H.*; Chesini, G.*; Serrao, V. A.; Franco, M. A. R.; **Cordeiro, C. M. B.***

In this paper, we propose a way to simplify the design of microstructured optical fibres with high sensitivity to applied pressure. The use of a capillary fibre with an embedded core allows the exploration of the pressure-induced material birefringence due to the capillary wall displacements and the photoelastic effect.

An analytical description of pressure-induced material birefringence is provided, and fibre modal characteristics are explored through numerical simulations. Moreover, a capillary fibre with an embedded core is fabricated and used to probe pressure variations. Even though the embedded-core fibre has a non-optimized structure, measurements showed a pressure sensitivity of (1.04 +/- 0.01(nm/bar, which compares well with more complex, specially designed fibre geometries reported in the literature. These results demonstrate that this geometry enables a novel route towards the simplification of microstructured fibre-based pressure sensors.

SCIENTIFIC REPORTS 7, 2990, 2017. DOI: 10.1038/s41598-017-03206-w

[P177-2017] "Spin Polarization of Carriers in InGaAs Self-Assembled Quantum Rings Inserted in GaAs-AlGaAs Resonant Tunneling Devices"

Gordo, V. O.; Gobato, Y. G.; Galeti, H. V. A.; B**rasil, M. J. S. P.***; Taylor, D.; Henini, M.

In this work, we have investigated transport and polarization resolved photoluminescence (PL) of n-type GaAs-AlGaAs resonant tunneling diodes (RTDs) containing a layer of InGaAs self-assembled quantum rings (QRs) in the quantum well (QW). All measurements were performed under applied voltage, magnetic fields up to 15 T and using linearly polarized laser excitation. It was observed that the QRs' PL intensity and the circular polarization degree (CPD) oscillate periodically with applied voltage under high magnetic fields at 2 K. Our results demonstrate an effective voltage control of the optical and spin properties of InGaAs QRs inserted into RTDs.

JOURNAL OF ELECTRONIC MATERIALS 46[7], 3851-3856, 2017. DOI: 10.1007/s11664-017-5391-2

[P178-2017] "Suppression of gamma(1S), gamma(2S), and gamma(3S) quarkonium states in PbPb collisions at root S--NN=2.76TeV"

Khachatryan, V.; Sirunyan, A. M.; Tumasyan, A.; C**hinellato, J. A.*; Tonelli Manganote, E. J.***; et al.
CMS Collaboration

The production yields of gamma(1S), gamma(2S), and gamma(3S) quarkonium states are measured through their decays into muon pairs in the CMS detector, in PbPb and pp collisions at the centre-of-mass energy per nucleon pair of 2.76TeV. The data correspond to integrated luminosities of 166 mu b(-1) and 5.4 pb(-1) for PbPb and pp collisions, respectively. Differential production cross sections are reported as functions of gamma rapidity y up to 2.4, and transverse momentum PT up to 20 GeV/c. A strong centrality-dependent suppression is observed in PbPb relative to pp collisions, by factors of up to approximate to 2 and 8, for the gamma(1S) and gamma(2S) states, respectively. No significant dependence of this suppression is observed as a function of y or PT. The gamma(3S) state is not observed in PbPb collisions, which corresponds to a suppression for the centrality-integrated data by at least a factor of approximate to 7 at a 95% confidence level. The observed suppression is in agreement with theoretical scenarios modeling the sequential melting of quarkonium states in a quark gluon plasma.

PHYSICS LETTERS B 770, 357-379, 2017. DOI: 10.1016/j.physletb.2017.04.031

[P179-2017] "Synthesis and magnetic properties of cobalt--iron/cobalt-ferrite soft/hard magnetic core/shell nanowires"

Londono-Calderon, C. L.; **Moscoso-Londono, O.*; Muraca, D.*; Arzuza, L.*; Carvalho, P.*; Pirota, K. R.*; Knobel, M.*;** Pampillo, L. G.; Martinez-Garcia, R.

A straightforward method for the synthesis of CoFe2.7/CoFe2O4 core/shell nanowires is described. The proposed method starts with a conventional pulsed electrodeposition procedure on alumina nanoporous template. The obtained CoFe2.7 nanowires are released from the template and allowed to oxidize at room conditions over several weeks. The effects of partial oxidation on the structural and magnetic properties were studied by x-ray spectrometry, magnetometry, and scanning and transmission electron microscopy. The results indicate that the final nanowires are composed of 5 nm iron-cobalt alloy nanoparticles. Releasing the nanowires at room conditions promoted surface oxidation of the nanoparticles and created a CoFe2O4 shell spinel-like structure. The shell avoids internal oxidation and promotes the formation of bi-magnetic soft/hard magnetic core/shell nanowires. The magnetic properties of both the initial single-phase CoFe2.7 nanowires and the final core/shell nanowires, reveal that the changes in the properties from the array are due to the oxidation more than effects associated with released processes (disorder and agglomeration).

NANOTECHNOLOGY 28[24], 245605, 2017. DOI: 10.1088/1361-6528/aa7010

[P180-2017] "The friendship paradox in species-rich ecological networks: Implications for conservation and monitoring"

Pires, M. M.; **Marquitti, F. M. D.***; Guimaraes, P. R.

A great challenge in ecology and conservation biology is to deal with the inherent complexity of ecological systems. Because species are embedded in species-rich systems characterized by multiple interactions, it is often hard to identify which species are really important for ecological processes such as pollination. Here we show that species-rich networks describing plant-pollinator interactions share a property with networks depicting social relationships, the friendship paradox, which allows identifying highly-connected species without detailed information on the whole network of interactions. Numerical simulations support that the identified species are those more likely to affect community structure and ecological dynamics. A sampling protocol taking into account the friendship paradox property could be adapted to field studies, helping in the search for conservation surrogates or to monitor changes in the communities, such as functional extinction or the increase in ecological importance of invasive species. We hypothesize that the friendship paradox is likely to arise in networks describing other types of ecological interactions. Besides being useful for conservation and ecosystem management, the friendship paradox may have relevant implications in other areas of biology as well.

BIOLOGICAL CONSERVATION 209, 245-252, 2017. DOI: 10.1016/j.biocon.2017.02.026

[P181-2017] "Thermodynamic Equilibria in Carbon Nitride Photocatalyst Materials and Conditions for the Existence of Graphitic Carbon Nitride g-C3N4"

Botari, T.*; Huhn, W. P.; Lau, V. W. H.; Lotsch, B. V.; Blum, V.

We quantify the thermodynamic equilibrium conditions that govern the formation of crystalline heptazine-based carbon nitride materials, currently of enormous interest for photocatalytic applications including solar hydrogen evolution. Key phases studied include the monomeric phase melem, the 1D polymer melon, and the hypothetical hydrogen free 2D graphitic carbon nitride phase "g-C3N4". conditions represented by the chemical potential of NH3.

Our study is based on. density functional theory including van der Waals dispersion terms with different experimental Graphitic carbon nitride is the subject of a vast number of studies, but its existence is still controversial. We show that typical conditions found in experiments pertain to the polymer melon (2D planes of 1D hydrogen-bonded polymer strands). In contrast, equilibrium synthesis of heptazine (h)-based g-h-C3N4 below its experimentally known decomposition temperature requires much less likely conditions, equivalent to low NH3 partial pressures around 1 Pa at 500 degrees C and around 10(3) Pa even at 700 degrees C. A recently reported synthesis of triazine (t)-based g--t-C3N4 in a salt melt is interpreted as a consequence of the altered local chemical environment of the C3N4 nanocrystallites.

CHEMISTRY OF MATERIALS 29[10], 4445-4453, 2017. DOI: 10.1021/acs.chemmater.7b00965

[P182-2017] "Tunable magnetocaloric effect around room temperature by Fe doping in Mn0.98Cr(0.02-x)FexAs compound"

Ipus, J. J.; Ribeiro, P. O.; von Ranke, P.; Vivas, R. J. C.; Carvalho, A. M. G.; **Coelho, A. A.***; Franco, V.; Rocco, D. L.

In this work, we present an investigation of the magnetic and magnetocaloric properties of Mn0.98Cr((0.02-x))FexAs compounds with x = 0.002, 0.005 and 0.010. Our findings show that as Fe content increases the unit cell volume decreases, which indicates that Fe doping emulates the pressure effect on the crystalline structure. The transition temperature T-C decreases as x increases and it can be set at approximate value of room temperature by changing the doping level. In addition, the magnetic entropy change Delta S-M was determined using a discontinuous measurement protocol, and realistic values from the magnetocaloric effect presented by MnAs-type compounds under pressure (emulated pressure) could be obtained. The values of Delta S-M(MAX) are very large, around -11 J kg(-1) K-1 with Delta H = 15 kOe, which is higher than that observed for most compounds with TC around room temperature. However, Delta S-M is confined to a narrow temperature range of 11 K. To overcome this drawback, the composition of a theoretical composite formed by our samples was calculated in order to obtain a table-shaped Delta S-M curve. The simulated composite showed a high value of full width at half maximum delta T--FWHM of 33 K, which is much higher than that of single sample.

JOURNAL OF MAGNETISM AND MAGNETIC MATERIALS 436, 85-90, 2017. DOI: 10.1016/j.jmmm.2017.04.030

[P183-2017]"Ultra-low-loss on-chip resonators with sub--milliwatt parametric oscillation threshold"

Ji, X.; **Barbosa, F. A. S.*;** Roberts, S. P.; Dutt, A.; Cardenas, J.; Okawachi, Y.; Bryant, A.; Gaeta, A. L.; Lipson, M.

On-chip optical resonators have the promise of revolutionizing numerous fields, including metrology and sensing; however, their optical losses have always lagged behind those of their larger discrete resonator counterparts based on crystalline materials and silica microtoroids. Silicon nitride (Si3N4) ring resonators open up capabilities for frequency comb generation, optical clocks, and high-precision sensing on an integrated platform. However, simultaneously achieving a high quality factor (Q) and high confinement in Si3N4 (critical for nonlinear processes, for example) remains a challenge. Here we show that addressing surface roughness enables overcoming the loss limitations and achieving high-confinement on-chip ring resonators with Q of 37 million for a ring of 2.5 mu m width and 67 million for a ring of 10 mu m width. We show a clear systematic path for achieving these high Qs, and these techniques can also be used to reduce losses in other material platforms independent of geometry. Furthermore, we demonstrate optical parametric oscillation using the 2.5 mu m wide ring with sub-milliwatt pump powers and extract the loss limited by the material absorption in our films to be 0.13 +/- 0.05 dB/m, which corresponds to an absorption-limited Q of at least 170 million by comparing two resonators with different degrees of confinement. Our work provides a chip-scale platform for applications such as ultralow-power frequency comb generation, laser stabilization, and sideband-resolved optomechanics.

OPTICA 4[6], 619-624, 2017. DOI: 10.1364/OPTICA.4.000619

[P184-2017] "Ultrahigh-Q optomechanical crystal cavities fabricated in a CMOS foundry"

Benevides, R.*; Santos, F. G. S.*; Luiz, G. O.*; Wiederhecker, G. S.*; Alegre, T. P. M.*

Photonic crystals use periodic structures to create frequency regions where the optical wave propagation is forbidden, which allows the creation and integration of complex optical functionalities in small footprint devices. Such strategy has also been successfully applied to confine mechanical waves and to explore their interaction with light in the so-called optomechanical cavities. Because of their challenging design, these cavities are traditionally fabricated using dedicated high-resolution electron-beam lithography tools that are inherently slow, limiting this solution to small-scale or research applications. Here we show how to overcome this problem by using a deep-UV photolithography process to fabricate optomechanical crystals in a commercial CMOS foundry. We show that a careful design of the photonic crystals can withstand the limitations of the photolithography process, producing cavities with measured intrinsic optical quality factors as high as Q(i) = (1.21 +/- 0.02) x 10(6). Optomechanical crystals are also created using phononic crystals to tightly confine the GHz sound waves within the optical cavity, resulting in a measured vacuum optomechanical coupling rate of g(0) = 2 pi x (91 +/- 4) kHz. Efficient sideband cooling and amplification are also demonstrated since these cavities are in the resolved sideband regime. Further improvements in the design and fabrication process suggest that commercial foundry-based optomechanical cavities could be used for quantum ground-state cooling.

SCIENTIFIC REPORTS 7, 2491, 2017. DOI: 10.1038/s41598-017-02515-4

[P185-2017] "X-ray dynamical diffraction in amino acid crystals: a step towards improving structural resolution of biological molecules via physical phase measurements"

Morelhao, S. L.; Remedios, C. M. R.; **Calligaris, G. A.***; Nisbet, G.

In this work, experimental and data analysis procedures were developed and applied for studying amino acid crystals by means of X-ray phase measurements. The results clearly demonstrated the sensitivity of invariant triplet phases to electronic charge distribution in D-alanine crystals, providing useful information for molecular dynamics studies of intermolecular forces. The feasibility of using phase measurements to investigate radiation damage mechanisms is also discussed on experimental and theoretical grounds.

JOURNAL OF APPLIED CRYSTALLOGRAPHY 50, 689-700, 2017. DOI: 10.1107/S1600576717004757

Eventos publicados

[P186-2017] "Intra and inter-channel nonlinearity compensation in WDM coherent optical OFDM using artificial neural network based nonlinear equalization"

Giacoumidis, E.; Mhatli, S.; Wei, J. L.; Le, S. T.; **Aldaya, I.*;** Stephens, M. F. C.; MacCarthy, M. E.; Ellis, A. D.; Doran, N. J.; Eggleton, B. J.
IEEE

Nonlinear effects are experimentally tackled, for the first time, in WDM-CO-OFDM by an artificial neural network (ANN)-based equalizer at 3200 km. For the middle 20-Gb/s channel ANN outperforms to Volterra-based equalization by similar to 2-dB in Q-factor.

Optical Fiber Communications Conference and Exhibition (OFC), MAR 19-23, 2017, Los Angeles, CA, 2017.

[P187-2017] "The DarkSide Experiment: Present Status and Future"

Zuzel, G.; Agnes, P.; Albuquerque, I. F. M.; **Segreto, E.*;** et al. Editado por: Galper A.; Petrukhin A.; Taranenko A.; Selyuzhenkov I.; Skorokhvatov M.; Rubin S.; Dmitrenko V.; Gurov Y.

DARKSIDE is a multi-stage program devoted to direct searches of Dark Matter particles with detectors based on double phase liquid Argon Time Projection Chamber. The DARKSIDE-50 setup is running underground at the Laboratori Nazionali del Gran Sasso. First it was operated with Atmospheric Argon and during that run (1422 +/- 67) kgxd of truly background--free exposure has been accumulated. Obtained data made it possible to set a 90% C.L. upper limit on the WIMP-nucleon cross section of 6.1 x 10(-44) cm(2) (for a WIMP mass of 100 GeV/c(2)). Presently the detector is filled with Underground Argon, which is depleted in Ar-39 by a factor of (1.4 +/- 0.2) x 10(3) with respect to Atmospheric Argon. Acquired so far (2616 +/- 43) kgxd (71 live days) in combination with the data from the Atmospheric Argon run give us the 90% C.L. upper limit on the WIMP-nucleon spin-independent cross section of 2.0 x 10(-44) cm(2) for a WIMP mass of 100 GeV/c(2). Up to date this is the best limit obtained with an argon target.

INTERNATIONAL CONFERENCE ON PARTICLE PHYSICS AND ASTROPHYSICS. Journal of Physics Conference Series, 798, UNSP 012109, 2017. DOI: 10.1088/1742-6596/798/1/012109

2nd International Conference on Particle Physics and Astrophysics (ICPPA), OCT 11-14, 2016, Moscow, RUSSIA, 2016.

Correções

[Co001-2017] "Centrality dependence of high-p(T) D-meson suppression in Pb-Pb collisions at root s(NN) = 2.7 6 TeV (vol 2015, 2015)"

Adam, J.; Adamova, D.; Aggarwal, M. M.; **Albuquerque, D. S. D.*; Chinellato, D. D.*; De Souza, R. D.*; Takahashi, J.*;** et al. ALICE Collaboration

This is an addendum to the article JHEP 11 (2015) 205 [1]. The figures 3 (right), 4 (right) and 5 are updated with published results on non--prompt J/psi-meson production from the CMS collaboration [2].

JOURNAL OF HIGH ENERGY PHYSICS 6, 032, 2017. DOI: 10.1007/JHEP06(2017)032

***Autores da comunidade IFGW**
Fonte: Web of Science on-line.

Defesas de Dissertações

[D006-2017] "Efeitos da dinâmica da nanopartícula catalisadora e controle da direção de crescimento de nanofios semicondutores"
Aluno: Mariana Zavarize Nica
Orientador: Profa. Dra. Mônica Alonso Cotta
Data: 28/07/2017

[D007-2017] "Estudo da atividade solar com detectores de partículas situados em solo terrestre"
Aluno: Henrique Vieira de Souza
Orientador: Prof. Dr. Anderson Campos Fauth
Data: 23/08/2017

[D008-2017] "Estrutura e dinâmica de contornos de grão no gelo"
Aluno: Ingrid de Almeida Ribeiro
Orientador: Prof. Dr. Maurice de Koning
Data: 25/08/2017

[D009-2017] "Fabricação e caracterização de filme fino regenerável hidrofóbico"
Aluno: Kally Chein Sheng Ly
Orientador: Prof. Dr. Antonio Riul Jr.
Data: 28/08/2017

[D010-2017] "Elaboração de um método global de reconstrução de chuveiros extensos utilizando otimização matemática"
Aluno: Yugo Mafra Kuno
Orientador: Prof. Dr. José Augusto Chinellato
Data: 28/08/2017

Defesas de Teses

[T016-2017] "Investigação das características físico-químicas da bactéria Xylella fastidiosa e seus biofilmes"
Aluno: Duber Marcel Murillo Munar
Orientador: Profa. Dra. Mônica Alonso Cotta
Data: 31/07/2017

[T017-2017] "Dinâmica de micro-osciladores acoplados"
Aluno: Gustavo de Oliveira Luiz
Orientador: Prof. Dr. Gustavo Silva Wiederhecker
Data: 05/09/2017

Fonte: Portal IFGW/Pós-graduação - Agenda de Colóquios, Defesas e Seminários.
Disponível em: http://portal.ifi.unicamp.br/pos-graduacao

Patentes

[Pa002-2017] "Multicamadas de SiO2 e de quantum dots de PbTe para dispositivo óptico chaveador"
Eugenio Rodriguez Gonzalez; Luiz Carlos Barbosa; Carlos Lenz Cesar
Número da Patente ou Registro: Agência INOVA: PI0500451-9
Tipo: Patente de Invenção
Mês/Ano de Conclusão: 08/2017 - INPI/BBRASIL

Fonte: SIPEX - Sistema de Informação de Pesquisa e Extensão da Unicamp.

O **Abstracta** é um boletim bimestral destinado à divulgação da produção científica da comunidade do Instituto de Física "Gleb Wataghin" - IFGW da Universidade Estadual de Campinas - Unicamp.

Fique por dentro!
Cadastre-se como leitor, e receba aviso da publicação de novos números por e-mail:
http://abstracta.ifi.unicamp.br

Abstracta

Instituto de Física
Diretor: Prof. Dr. Pascoal José Giglio Pagliuso
Diretora Associada: Profa. Dra. Mônica Alonso Cotta
Universidade Estadual de Campinas - UNICAMP
Cidade Universitária Zeferino Vaz
13083-859 - Campinas - SP - Brasil
e-mail: secdir@ifi.unicamp.br

Publicação

Biblioteca do Instituto de Física Gleb Wataghin
http://portal.ifi.unicamp.br/biblioteca

Diretora Técnica: Sandra Maria Carlos Cartaxo
Coordenador da Comissão de Biblioteca: Prof. Dr. André Koch Torres de Assis

Elaboração
Maria Graciele Trevisan (Bibliotecária)
Ayres Neri da Cunha Junior (Técnico Administrativo)
contato: infobif@ifi.unicamp.br